Evolution of the isotropic-to-nematic phase transition in octyloxycyanobiphenyl+aerosil dispersions

A. Roshi and G. S. Iannacchione
Department of Physics, Worcester Polytechnic Institute, Worcester, Massachusetts 01609, USA

P. S. Clegg and R. J. Birgeneau
Department of Physics, University of Toronto, Toronto, Ontario, Canada M5S 1A7

(Received 1 October 2003; published 15 March 2004)

High-resolution ac calorimetry has been carried out on dispersions of aerosils in the liquid crystal octyloxycyanobiphenyl (8OCB) as a function of aerosil concentration and temperature spanning the crystal to isotropic phases. The liquid crystal 8OCB is elastically stiffer than the previously well studied octylcyanobiphenyl (8CB)+aerosil system and so general quenched random-disorder effects and liquid crystal specific effects can be distinguished. A double heat capacity feature is observed at the isotropic to nematic phase transition with an aerosil independent overlap of the heat capacity wings far from the transition and having a nonmonotonic variation of the transition temperature. A crossover between low and high aerosil density behavior is observed for 8OCB+aerosil. These features are generally consistent with those on the 8CB+aerosil system. Differences between these two systems in the magnitude of the transition temperature shifts, heat capacity suppression, and crossover aerosil density between the two regimes of behavior indicate a liquid crystal specific effect. The low aerosil density regime is apparently more orientationally disordered than the high aerosil density regime, which is more translationally disordered. An interpretation of these results based on a temperature dependent disorder strength is discussed. Finally, a detailed thermal hysteresis study has found that crystallization of a well homogenized sample perturbs and increases the disorder for low aerosil density samples but does not influence high-density samples.

DOI: 10.1103/PhysRevE.69.031703 PACS number(s): 64.70.Md, 61.30.Eb, 65.40.Ba

I. INTRODUCTION

The effect of quenched random disorder on phase structure and transitions is an important area of study that continues to attract a great deal of research. Disorder is ubiquitous (ideal pure transitions being the exception rather than the rule in nature) and the effect on phase transitions can be profound. Phase transitions are modified depending on the aspect of the system affected by the disorder, on the dimensionality, and on the number of components to the order parameter. Of particular interest is a linear coupling between quenched random disorder and the order parameter, which allows for a random-field theoretical approach. Also, the order of the transition is crucial as first-order transitions have additional considerations compared to continuous transitions. This is due to the presence of two-phase coexistence (hence interfaces between ordered and disordered regions), intrinsically finite correlation length at the transition, and hysteresis effects for first order compared to continuous phase transitions. This has made the experimental and theoretical studies of quenched random-disorder effects at first-order transitions challenging.

Liquid crystals (LC) are a particularly attractive system for the study of phase transitions into partially ordered phases. This makes them especially interesting for the study of the effects of quenched random disorder (QRD), which are typically introduced by the random fixed dispersion of solid surfaces. In LC+aerosil systems, the quenched random disorder is created by a dispersed gel of aerosil particles and is varied by changing the density of aerosils in the dispersion. A convenient measure of the introduced disorder is the grams of silica per cubic centemeter of liquid crystal, denoted the conjugate silica density ρ_S, which is directly related to the surface area of solids as well as the mean distance between solid surfaces [1,2]. The aerosils used are silica spheres that can hydrogen bond together to form a fractal-like random gel. Studies have previously been carried out by various groups on liquid crystals in an aerogel medium [3]. Aerogels are self-supporting structures and this places a lower limit on the disorder strength that can be probed. By contrast, the aerosil gel provides a weaker and more easily controlled perturbation, and thus opens up a physically interesting regime.

In this work, we study the effect of quenched random disorder due to a dispersed thixotropic aerosil gel on the weakly first-order isotropic to nematic (I-N) phase transition. The calorimetric results for the nematic to smectic-A phase transition in octyloxycyanobiphenyl 8OCB+aerosil samples have been previously reported and were shown to be consistent with results in 8CB+aerosil samples [4]. At the I-N transition, the orientational order has a finite correlation length and is established in three dimensions, which is describable by a symmetric and traceless second-rank tensor Q_{ij} [5] (as such, it possesses only five independent components). Thus, nematic order belongs, in principle, to a $d=3$, $n=5$ Heisenberg class. However, by ignoring any biaxial character and aligning the orientation axis with a principle axis of a local frame, this tensor can be split into a scalar order parameter S measuring the magnitude of orientational order about the orientation axis and a ''headless'' vector called the nematic director $\hat{n}$ ($\hat{n}=-\hat{n}$) describing the spatial

orientation of this axis. In this simplified view, nematic order is described on short length scales by S and on longer length scales by $\hat{n}$, which is useful in describing the elastic properties of the nematic structure. These measures of nematic order are related to the quadrupolar nematic order parameter by $Q_{ij}=\frac{1}{2}S(3\hat{n}_i\hat{n}_j-\delta_{ij})$.

In principle, the effect of the aerosil gel network on the orientational order of the nematic phase is twofold. The silica gel first dilutes the liquid crystal and second creates a preferred local orientation [6,7]. In addition, the first-order transition from the isotropic to the nematic phase necessitates the formation of interfaces between coexisting domains/phases, which must occur within the available void spaces. The latter effect is the classic result of quenched random disorder, a distribution of transition temperatures due to the nucleation of ordered domains within voids having some size distribution. This leads to short-range order (SRO), a rounding of the transition, and suppression of the first-order character of the transition [8]. The contribution of a random preferred local orientation effect to the total Hamiltonian can be represented as

$$\mathcal{H}_{rf}=-\sum_i g_2(h_i\cdot\hat{n}_i)^2, \tag{1}$$

where $\hat{\mathbf{n}}_i$ is the orientation of the molecules over some small region where the orientation is approximately constant and $\mathbf{h}_i$ is the random influence of the silica surface. The variance of this random field $\langle h^2\rangle$ should be proportional to the density of solids dispersed in the LC medium. This term is squared due to the effective inversion symmetry of the molecules in the nematic phase. Since the nematic order parameter is quadratic in $\hat{\mathbf{n}}_i$ due to the same inversion symmetry [5], Eq. (1) is also linear in the order parameter and hence constitutes a random-field (RF) interaction. Recently, Eq. (1) has also been interpreted as a random-anisotropy interaction [7] but this seems only applicable to systems describable by a pure vector $n=3$ order parameter. The formation of interfaces and the resulting surface energy penalties places restrictions on the effects of $\langle h^2\rangle$ depending on the elasticity of the nematic. Light-scattering measurements have shown that the nematic phase in liquid crystal and aerosil dispersions breaks up into large (micron size) but finite-size domains [9]. In addition, more extensive optical studies focussing on the nature of the nematic director structure well below the I-N transition have shown that the director correlation length $\xi_{\hat{n}}$ decays exponentially with distance, which is a hallmark of short-range order [10,11]. These features are consistent with an RF interaction for nematics with QRD.

To date, the most thoroughly studied LC+aerosil system is the dispersion of type-300 aerosil in octylcyanobiphenyl (8CB), denoted 8CB+aerosil. Detailed calorimetric [1,12,13], x-ray scattering [14,15], x-ray intensity fluctuation spectroscopy [16], static and dynamic light scattering [9–11], and deuterium nuclear magnetic resonance (NMR) [17] studies on the nematic to smectic-A (N–Sm-A) and the isotropic to nematic (I-N) phase transitions of this system have shown that there are clear quenched random-field characteristics as well as finite-size scaling effects [2].

Calorimetry measurements on 8CB+aerosil samples have been particularly useful in yielding detailed information on both the I-N and the N–Sm-A phase transitions [1]. The results for both transitions show a complex dependence of the transition temperature on the aerosil density. While the N–Sm-A heat capacity peak remains sharp and evolves towards three-dimensioanl (3D)-XY behavior with increasing silica density, the I-N behavior is more complicated. For silica densities below $\rho_S\sim 0.1\ \mathrm{g\,cm^{-3}}$, two heat capacity peaks, closely spaced in temperature, were observed. At higher aerosil densities, the heat capacity peaks for both the I-N and the N–Sm-A transitions displayed a highly smeared and nonsingular features. Deuterium NMR (DNMR) measurements on deuterated 8CB+aerosil dispersions, which were carried out over a wide range of silica densities, showed that the magnitude of the orientational order S below the I-N transition temperature was essentially unchanged from bulk behavior [17]. The amount of liquid crystal reorientation for field-cooled samples upon rotation within the DNMR field is small and decreases continuously with silica density up to $\rho_S=0.094\ \mathrm{g\,cm^{-3}}$ (the units will be dropped hereafter) confirming distinct low and high ρ_S behavior. An x-ray intensity fluctuation spectroscopy (XIFS) study have found evidence of aerosil gel dynamics in 8CB+aerosil dispersions indicating an elastic coupling between the gel and LC [16]. The optical, calorimetric, DNMR, and XIFS results all appear to be consistent with a model in which director fluctuations are suppressed with increasing aerosil density.

The present work focusses on a different liquid crystal—8OCB—having dispersed in it the same type of aerosil over a comparable range of silica densities as the well-studied 8CB+aerosil system. This liquid crystal has several important differences from the closely related 8CB. The liquid crystal 8OCB has stronger smectic and nematic interactions than 8CB as evidenced by the higher transition temperatures, the larger bare correlation lengths for smectic interactions [18], and the larger elastic constants. More specifically, 8OCB has a 17% larger bend, 36% larger twist, and 10% larger splay nematic elastic constants than 8CB (in the single elastic constant approximation, 8OCB has a $\approx$20% greater K_N than 8CB with an overall uncertainty of 5%) [19]. Thus, comparison of behaviors between 8CB+aerosil and 8OCB +aerosil systems allow for the isolation of general QRD effects from material specific effects, in this case the elasticity of the liquid-crystal host medium.

In general, this work reveals a nonmonotonic silica density dependence of the I-N and N–Sm-A transition temperatures similar to that observed for 8CB+aerosil but occurring over a larger ρ_S range for 8OCB+aerosil. The calorimetric results presented here for the I-N transition reveal the onset of a double transition peak for $\rho_S>0.1$ with a ρ_S dependence on the temperature distance between the two heat capacity peaks. Evidence is presented that the first-order character of the I-N transition continuously decreases with silica content, becoming approximately zero for $\rho_S\gtrsim 0.7$. Over the entire range of ρ_S studied here, the heat capacity temperature dependence away from the immediate vicinity of the transition region is bulklike and independent of silica content.

We speculate that the variance of the disorder $\langle h^2 \rangle$ may change through a first-order transition for nematics to account for these observations. Such a variation of the disorder strength may be due to the silica surfaces introducing a low-order, paranematiclike, boundary layer initially screening the remaining liquid crystal material. The thickness of this boundary layer is strongly temperature dependent in the immediate vicinity of the *I*-*N* transition and as it shrinks, the screening becomes weaker.

Section II describes the preparation of the 8OCB+aerosil dispersions as well as the ac-calorimetry technique employed. Given in Sec. III is a presentation of the results. All results are then discussed in Sec. IV and related to results from previous LC+aerosil studies. Directions for future study will also be discussed.

II. EXPERIMENTAL TECHNIQUES

The liquid crystal 8OCB, purchased from Aldrich, was used after degassing in the isotropic phase for 1 h. This liquid crystal molecule has an aliphatic tail attached by an oxygen link to the rigid biphenyl core and a polar cyano head group ($M_w = 307.44$ g mol^{-1}). This oxygen link constitutes the sole molecular difference between 8OCB and 8CB. Pure 8OCB has a weakly first-order isotropic to nematic transition at $T^o_{I\text{-}N} \sim 353$ K and a second-order nematic to smectic-*A* transition at $T^o_{N\text{-}A} \sim 340$ K. At lower temperatures, the strongly first-order crystal–Sm-*A* transition occurs reproducibly on heating at $T^o_{Cr\text{-}A} \sim 328$ K and, as usual, can be greatly supercooled.

The hydrophilic type-300 aerosil obtained from Degussa [20] was thoroughly dried at ~300 °C under vacuum for a couple of hours prior to use. The hydrophilic nature of the aerosils arises from the hydroxyl groups covering the surface and allows the aerosil particles to hydrogen bond to each other. This type of bonding is weak and can be broken and reformed, which leads to the thixotropic nature of gels formed by aerosils in an organic solvent. Crystallization severely disrupts the gel. The specific surface area measured by the manufacturer via Brunauen-Emmett-Teller nitrogen isotherms is 300 m^2 g^{-1} and each aerosil sphere is roughly 7 nm in diameter. However, small-angle x-ray scattering (SAXS) studies have shown that the basic aerosil unit consists of a few of these spheres fused together during the manufacturing process [1]. Each 8OCB+aerosil sample was created by mixing appropriate quantities of liquid crystal and aerosil together, then dissolving the resulting mixture in spectroscopic grade (low water content) acetone. The resulting solution was then dispersed using an ultrasonic bath for about 1 h. As the acetone evaporates from the mixture, a fractal-like gel forms through diffusion-limited aggregation. Small-angle x-ray studies have shown that the aerosil gel dispersion has a fractal structure and no preferred orientation [1] on the micron-long length scales of nematic order [10].

At room temperature, 8OCB is a crystalline solid even in the presence of high aerosil density. Care was taken to avoid crystallization of 8OCB and possible damage to the aerosil gel, especially for low silica densities. For this calorimetry study, the mixture after slow solvent evaporation was allowed to crystallize, and the solid sample was transferred into the calorimetry cell. The cell was then sealed, the heater and thermometer attached, and the cell was heated into the isotropic phase. The sample was then remixed by placing the assembly in an ultrasonic bath for over 1 h. The cell and sample temperature was kept elevated during the mounting of the sealed cell into the calorimeter by maintaining current through the heater. This sample preparation protocol also allows a controlled entry into the crystal phase. However, since the cell is sealed, the *in situ* remix could not be inspected and so some small dispersion inhomogeneity may remain.

High-resolution ac calorimetry was performed using two homebuilt calorimeters at WPI. The sample cell consisted of a silver crimped-sealed envelope ~10 mm long, ~5 mm wide, and ~0.5 mm thick (closely matching the dimensions of the heater). After the sample was introduced into a cell having an attached 120-Ω strain-gauge heater and 1-MΩ carbon-flake thermistor, a constant current was placed across the heater to maintain the cell temperature well above $T_{I\text{-}N}$. The filled cell was then placed in an ultrasonic bath to remix the sample. After remixing, the cell was mounted in the calorimeter, the details of which have been described elsewhere [21]. In the ac mode, power is input to the cell as $P_{ac}e^{i\omega t}$ resulting in temperature oscillations with amplitude T_{ac} and a relative phase shift of $\varphi \equiv \Phi + \pi/2$, where Φ is the absolute phase shift between $T_{ac}(\omega)$ and the input power. Defining $C^* = P_{ac}/\omega|T_{ac}|$, the specific heat at a heating frequency ω is given by

$$C_p = \frac{[C'_{filled} - C_{empty}]}{m_{sample}} = \frac{C^* \cos(\varphi) f(\omega) - C_{empty}}{m_{sample}}, \quad (2)$$

$$C''_{filled} = C^* \sin(\varphi) g(w) - \frac{1}{\omega R_e}, \quad (3)$$

where C'_{filled} and C''_{filled} are the real and imaginary components of the heat capacity, C_{empty} is the heat capacity of the cell and silica, m_{sample} is the mass in grams of the liquid crystal (the total mass of the 8OCB+aerosil sample was ~20 mg, which yielded m_{sample} values in the range of 13–20 mg), and R_e is the external thermal resistance between the cell and the bath (here, ~200 K W^{-1}). The functions $f(\omega) \approx g(\omega) \approx 1$ are small correction factors to account for the non-negligible internal thermal resistance R_i of the sample and cell compared to R_e. These corrections were applied to all samples studied here [22]. Several frequency scans were performed in order to ensure the applicability of Eqs. (2) and (3) and to chose an operating ω such that C_p was independent of frequency. All data presented here were taken at $\omega = 0.1473$ s^{-1} at a scanning rate of less than ±100 mK h^{-1}, which yield essentially static C_p results [23]. All 8OCB +aerosil samples experienced the same thermal history after mounting; 6 h in the isotropic phase to ensure homogeneous gelation, then a slow cool deep into the smectic phase before beginning the first detailed scan upon heating followed by a detailed scan on cooling. The results from the cooling scans are completely consistent with those from heating and so only the heating scan results are shown in detail.

TABLE I. Summary of the calorimetric results for 8OCB+aerosil samples averaged from the heating and cooling scans. The sample density (ρ_S in g of aerosil per cm^3 of 8OCB) as well as the I-N/($T_{I\text{-}N}$) and the N–Sm-A (T^*) phase transition temperatures, the nematic range ($\Delta T_N = T_{I\text{-}N} - T^*$), the width of the I-N coexistence region ($\delta T_{I\text{-}N}$), and the difference in temperature between the two $\Delta C_p(IN)$ peaks (δT_{2p}) all in kelvins are shown. The I-N transition ac-enthalpy ($\delta H^*_{I\text{-}N}$) and the integrated imaginary specific heat ($\delta H''_{I\text{-}N}$) in J g^{-1} are also tabulated. The quoted error represent the maximum range of reproducibility from measurements at the same ρ_S but from different sample batches.

ρ_S	$T_{I\text{-}N}$	T^*	ΔT_N	$\delta T_{I\text{-}N}$	δT_{2p}	$\delta H^*_{I\text{-}N}$	$\delta H''_{I\text{-}N}$
0	352.47±0.10	339.52±0.34	12.95	0.10		6.57±0.66	0.25
0.036	352.56±0.18	339.64±0.34	12.92	0.11		6.69±0.67	0.19
0.051	352.75±0.25	340.22±0.61	12.56	0.32		7.17±0.72	0.24
0.078	351.03±0.18	338.61±0.34	12.42	0.27		6.88±0.69	0.10
0.105	351.02±0.25	338.51±0.68	12.51	0.18		7.03±0.70	0.12
0.220	351.16±0.17	338.61±0.34	12.55	0.27	0.09	7.08±0.71	0.12
0.347	352.30±0.18	338.85±0.34	13.45	0.46	0.11	6.96±0.70	0.08
0.489	352.17±0.18	338.05±0.68	14.12	0.70	0.22	6.77±0.68	0.04
0.647	351.09±0.25	337.30±0.92	13.79	1.20	0.54	6.22±0.62	0.01

III. RESULTS

A. General description

The heat capacity of the pure 8OCB liquid crystal is in good agreement with previously published results [24,25]. For our pure 8OCB material the transition temperatures were $T^o_{I\text{-}N} = 352.53$ K and $T^o_{N\text{-}A} = 339.52$ K. The I-N two-phase coexistence width was ≈ 95 mK wide, and the N–Sm-A transition enthalpy was $\delta H^o_{N\text{-}A} = 0.42$ J g^{-1}. These thermal features indicate that the 8OCB liquid crystal used in this study was of reasonably good quality. A summary of the calorimetric results for pure 8OCB and 8OCB+aerosil samples is given in Table I. Measurements were repeated in order to test the remixing procedure at several ρ_S on samples from different mixture batches and the quoted errors represent the maximum variation observed. This uncertainty is approximately two orders of magnitude larger than the ability to experimentally determine the temperature position of a specific heat feature.

In order to determine the excess heat capacity associated with the phase transitions, an appropriate background was subtracted. The total sample heat capacity over a wide temperature range had a linear background, $C_p^{\text{background}}$, subtracted to yield

$$\Delta C_p = C_p - C_p^{\text{background}} \tag{4}$$

as the excess C_p due to the I-N and N–Sm-A phase transitions. The resulting ΔC_p data are shown for pure 8OCB and all 8OCB+aerosil samples in Fig. 1 over a wide temperature range about $T_{I\text{-}N}$, where the units are J K^{-1} per gram of *liquid crystal*. The transition temperature $T_{I\text{-}N}$ is determined as the highest temperature where any nematic phase is present and corresponds to the highest temperature peak in C''_{filled} [26].

As seen in Fig. 1, the ΔC_p values away from the N–Sm-A transition and the $I+$N coexistence regions overlap with bulk behavior independent of silica concentration. The detailed variations of ΔC_p associated with the N–Sm-A transition with ρ_S has been reported previously [4]. The deviations of some of the $\rho_S = 0.05$ points in the nematic phase is likely a consequence of sample inhomogeneity. The ΔC_p "wings" of the I-N transition are associated with short-range fluctuations of nematic order. Given the simplification of the nematic order parameter, the short-range fluctuations in bulk nematics are mainly composed of thermal fluctuations of the scalar part S. For the 8OCB+aerosil system, the temperature dependence of $\Delta C_p(IN)$ being independent of ρ_S suggests that thermal fluctuations of S are independent of disorder over the whole range of ρ_S studied in this work. The $\Delta C_p(IN)$ wing behavior shown here for 8OCB+aerosil is completely consistent with similar results for 8CB+aerosil [1] and low-density 8CB+aerogel samples [27].

In stark contrast to the behavior of ΔC_p in the one-phase regions, the two-phase coexistence region of the I-N transi-

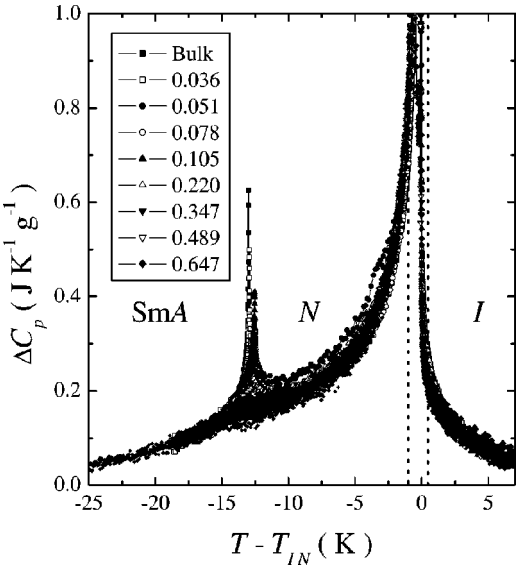

FIG. 1. Excess specific heat ΔC_p obtained on heating as a function of temperature about $T_{I\text{-}N}$ for bulk 8OCB and 8OCB+aerosil samples from $\rho_S = 0.036$ to 0.647 g of silica per cm^3 of liquid crystal. See figure inset for definition of symbols. The vertical dashed lines indicate the I-N transition region expanded in Fig. 2.

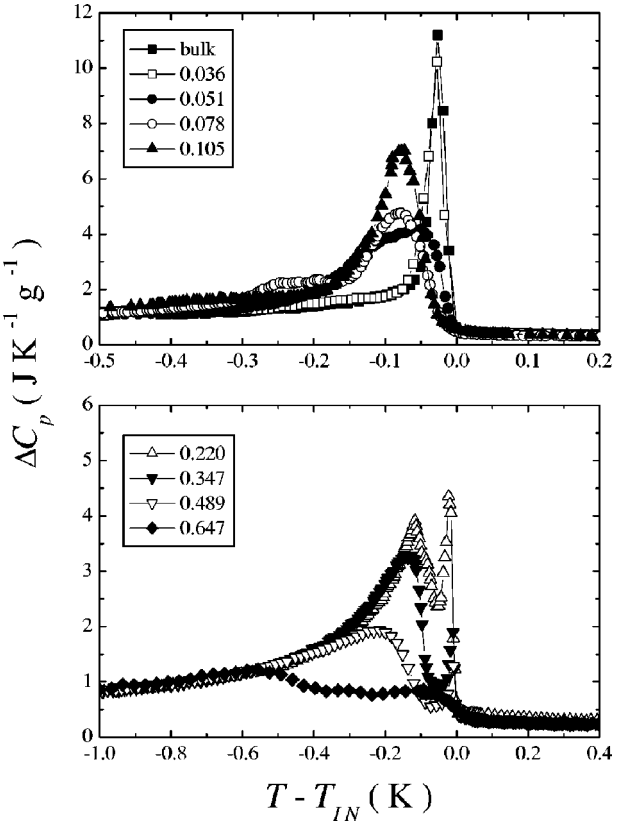

FIG. 2. Expanded view of the excess specific heat about the *I*-*N* transition as a function of temperature (all data obtained on heating). See figure insets for definition of symbols. The samples have been separated into two groups; the upper panel appears to indicate inhomogeneity induced broadening for samples with $\rho_S \lesssim 0.1$; the lower panel depicts the evolution of ΔC_p for $\rho_S > 0.1$ and shows two distinct features, one sharp and one broad feature consistent with those seen in 8CB+aerosil systems [1]. The upper panel has twice the *y*-axis range and half the *x*-axis range as the lower panel, thus both panels depict the same area in J g^{-1} units.

tion exhibits strong effects of silica concentration, as shown in Fig. 2. From 1 K below to 0.4 K above $T_{I\text{-}N}$, the $\Delta C_p(IN)$ peaks for the pure 8OCB and the $\rho_S = 0.036$ sample are essentially the same [28]. Upon increasing silica density, the peak in $\Delta C_p(IN)$ is substantially lower in temperature relative to the peak in C''_{filled} and considerably broader than for the bulk or the $\rho_S = 0.036$ sample. See the upper panel in Fig. 2. In addition, there is a small and very broad shoulder below the main specific heat peak, also seen in bulk, which moves toward the main peak with increasing ρ_S. The nature of this subsidiary feature is not known. It is likely, given the similarity of the materials used here with the 8CB+aerosil system, that the percolation threshold for type-300 aerosil in 8OCB is essentially the same at $\rho_P \approx 0.018$ [1] and so a true gel should be present for all samples studied in this work. This is supported by a visual inspection of these samples holding their shape above the crystal melting temperature. The *I*-*N* transition regions shown in Fig. 2 for $\rho_S \lesssim 0.1$ appear to be quite sensitive to small inhomogeneities in the silica gel dispersion and so are grouped together. Given the dominance of a large, broad, specific heat peak and relatively erratic transition temperature shifts, discussed below, the effect of the silica gel on the *I*-*N* phase transition is strongly dependent on the quality of the dispersion.

Beginning with the $\rho_S = 0.22$ sample and for increasing silica content there is a systematic variation of the excess heat capacity, which is shown by the lower panel in Fig. 2. At $\rho_S = 0.22$, a double heat capacity feature is observed with a sharp high-temperature peak ΔC_p^{HT} corresponding closely to (but very slightly below) a sharp peak in C''_{filled}, followed at lower temperature by a broader peak ΔC_p^{LT} also having an associated broad peak in C''_{filled}. Clearly, both are first-order signatures and they are separated by ≈ 0.1 K. For the $\rho_S = 0.347$ and 0.489 samples, the ΔC_p^{HT} feature remains sharp but decreases in magnitude while the ΔC_p^{LT} feature becomes increasingly rounded and moves to lower temperature relative to ΔC_p^{HT} by 0.15 and 0.2 K, respectively. For the $\rho_S = 0.647$ sample, both heat capacity features are rounded and separated now by ~ 0.5 K. Over this entire range of silica density, the size of the C''_{filled} peak decreased monotonically with increasing ρ_S. Such a double *I*-*N* heat capacity feature was observed in 8CB+aerosil samples for silica concentrations up to $\rho_S \approx 0.1$, but ΔC_p exhibited a single, rounded feature above this density [1]. Only a single rounded $\Delta C_p(I\text{-}N)$ feature was observed for all 8CB+aerogel samples [27].

B. The *I*-*N* transition enthalpies

The *I*-*N* transition enthalpy also exhibits a dependence on aerosil concentration and can be a quantitative measure of the strength of the transition. For a second-order (or continuous) phase transition, the change in enthalpy through the transition is given by

$$\delta H = \int \Delta C_p dT, \tag{5}$$

where the limits of integration are as wide as possible about the heat capacity peak. However, for first-order transitions the situation is complicated by the presence of a two-phase coexistence region, in this work $I+\mathrm{N}$, as well as a latent heat ΔH. The total enthalpy change through a first-order transition is the sum of the pretransitional enthalpy and the latent heat. In an ac-calorimetric measurement, ΔC_p values observed in the two-phase region are artificially high and frequency dependent due to partial phase conversion during a T_{ac} cycle. The pretransitional enthalpy δH is typically obtained by substituting a linearly truncated ΔC_p behavior between the bounding points of the two-phase coexistence region into Eq. (5), and an independent experiment is required to determine the latent heat ΔH [1]. A direct integration of the observed ΔC_p yields an effective transition enthalpy δH^* and this contains some of the latent heat contributions; thus $\delta H < \delta H^* < \Delta H_{total} = \delta H + \Delta H$. The uncertainty in determining the transition enthalpy from an ac-calorimetric measurement is typically 10%.

For our analysis, the observed $\Delta C_p(I\text{-}N)$ was directly integrated over a wide temperature range of -25 K below to $+5$ K above $T_{I\text{-}N}$ for all bulk and 8OCB+aerosil samples

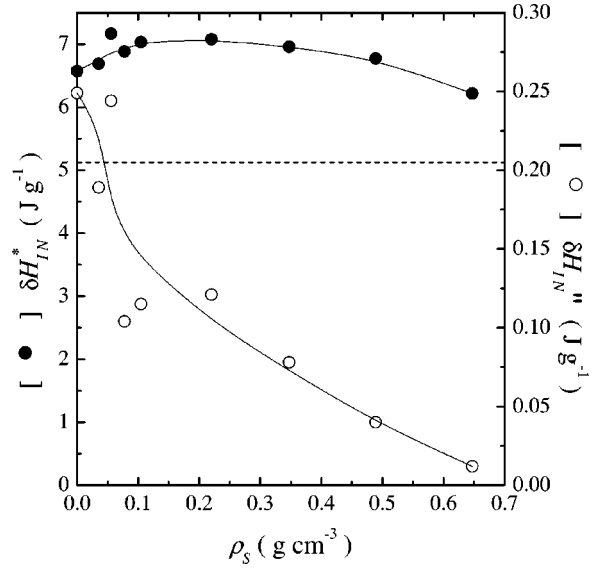

FIG. 3. The real (solid symbol, left axis) and imaginary (open symbol, right axis) I-N transition enthalpy are shown as a function of ρ_S. The effective enthalpy $\delta H^*_{I\text{-}N}$ is weakly dependent on silica content, indicating only minor changes to the latent heat conversion dynamics occur relative to the ac frequencies employed in this work. The monotonic decrease in the imaginary component is evidence that the first-order character of the I-N transition decreases with increasing quenched disorder. Solid lines are guides to the eye while the horizontal dotted line represents the total pretransitional enthalpy $\delta H_{I\text{-}N}=5.13$ J g^{-1}, which is independent of ρ_S. See text for details.

where the $N-$Sm-A transition enthalpy contribution was subtracted. This will be referred to hereafter as the ac-enthalpy and denoted as $\delta H^*_{I\text{-}N}$, as it represents only a part of the total transition enthalpy. As seen in Fig. 1, an integration of a linearly truncated $\Delta C_p(I\text{-}N)$ in the two-phase coexistence region over a similar range yields a pretransitional enthalpy $\delta H_{I\text{-}N}=5.13$ J g^{-1} that is independent of aerosil density. Integration over a similar temperature range yielded a pretransitional $\delta H_{I\text{-}N}$ value of 5.43 J g^{-1} for 8CB+aerosil samples, also independent of silica density [1]. In addition, the integration of the imaginary heat capacity given by Eq. (3) and normalized to the LC mass, defines an imaginary transition enthalpy, referred to as im-enthalpy and denoted as $\delta H''_{I\text{-}N}$, which is an indicator of the first-order character of the transition. Although $\delta H''_{I\text{-}N}$ is a measure of the dispersive component of the complex enthalpy, it is only approximately proportional to the transition latent heat due to the fixed-ω ac technique employed in this work. As the silica content changes, the two-phase conversion rate may change and so alter the proportionality between $\delta H''_{I\text{-}N}$ and $\Delta H_{I\text{-}N}$; thus a detailed frequency scan for each sample would be needed to fully characterize the relationship. This was done for a few samples and the frequency employed in this work is sufficiently close to the static limit that this effect should be minimal.

The results of both the ac- and im-enthalpy for 8OCB +aerosil samples are shown in Fig. 3 as a function of the silica density. There is a slight variation (first increasing for increasing ρ_S up to 0.220 then decreasing for larger ρ_S) of the ac-enthalpy due mainly to changes in ΔC_p values within the two-phase coexistence range since the heat capacity wings away from the transition are ρ_S independent (except for $\rho_S=0.051$, which is systematically high for $T-T_{I\text{-}N}$ from -3 K to -10 K). Given the fixed-ω aspect of the technique, any variation observed in the ac-enthalpy in the two-phase region can be attributable to changes in either the dynamics or magnitude (or both) of the latent heat evolution. The small nonmonotonic variation of $\delta H^*_{I\text{-}N}$ for 8OCB +aerosil samples is in contrast to the systematic decrease of $\delta H^*_{I\text{-}N}$ with increasing ρ_S for 8CB+aerosil samples. This may reflect a difference in the phase conversion dynamics between 8CB and 8OCB and how they are modified by the presence of aerosils.

The interpretation of the im-enthalpy is more straightforward as it is closely related to the latent heat of the transition. With increasing ρ_S, the im-enthalpy appears to monotonically decrease to almost zero for $\rho_S=0.647$, see Fig. 3. This suggests that for the highest ρ_S sample studied, the I-N latent heat has become nearly zero. Similar trends were observed for 8CB+aerosil [1] where a continuous I-N transition is estimated to occur near $\rho_S\approx 0.8$. Also, a nearly continuous I-N transition was reported for $7CB$+aerosil for silica densities near $\rho_S\approx 1$ as well as indications of a double feature at the I-N transition for $\rho_S\approx 0.1$ [29]. The above observations are consistent with the general view that with increasing QRD, first-order transitions are driven continuous [8].

C. Transition temperatures and crystallization

The I-N transition temperature, defined here as the peak in C''_{filled} for the highest-temperature feature, for the 8OCB +aerosil samples as well as those for the 8CB+aerosil system taken from Ref. [1] are shown in Fig. 4 as a function of silica density. For the 8OCB+aerosil system, $T_{I\text{-}N}$ is essentially unchanged up to $\rho_S=0.051$ then decreases sharply by $\sim$1.5 K at $\rho_S=0.078$, 0.105, and 0.220. It then rises strongly for $\rho_S=0.347$, nearly recovering the bulk value. Upon further increase in ρ_S, $T_{I\text{-}N}$ decreases monotonically (with a concave downward character) until it is again about $\sim$1.5 K below $T^o_{I\text{-}N}$ for the $\rho_S=0.647$ sample. The nonmonotonic evolution of $T_{I\text{-}N}$ with silica content for the 8OCB+aerosil system is similar to that seen in the 8CB+aerosil system, suggesting that the initial depression of $T_{I\text{-}N}$, recovery, then continued depression is a general phenomena of quenched random disorder on nematics while the specific ρ_S dependence is liquid crystal material dependent. Over this same range in silica density, the width of the two-phase coexistence region $\delta T_{I\text{-}N}$ also has a nonmonotonic dependence on ρ_S, as seen in Table I. However, $\delta T_{I\text{-}N}$ is sensitive to local inhomogeneities of the aerosil dispersion that may account for its variation when $\rho_S<0.1$. Beginning at $\rho_S=0.105$, $\delta T_{I\text{-}N}$ increases monotonically by a factor of $\sim$6.7 while ρ_S increases by a factor of $\sim$6. The observed broadening of the two-phase coexistence width is nearly in direct proportion with increasing QRD and is generally consistent with the behavior of first-order transitions with quenched disorder [8].

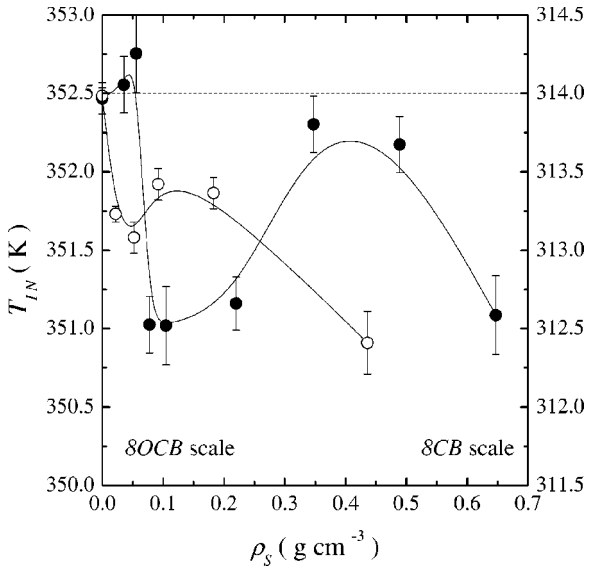

FIG. 4. Dependence on ρ_S of the I-N transition temperature $T_{I\text{-}N}$ for 8OCB+aerosil (solid circles and left axis, $T^o_{I\text{-}N}=352.47$ K) and 8CB+aerosil (open circles and right axis, $T^o_{I\text{-}N}=313.99$ K) samples. Data for 8CB+aerosil samples taken from Ref. [1]. Note that both the left and right axes span 3 K in temperature. The solid lines are guides to the eye.

The N–Sm-A pseudotransition temperatures T^* scaled by the bulk transition temperature $T^o_{N\text{-}A}$ for 8OCB+aerosil and 8CB+aerosil systems are shown in Fig. 5. The pattern of fractional changes in T^* is essentially the same for both LC+aerosil systems with an initial rapid depression, recovery, then more gradual decrease with a total change of less than 1% from $T^o_{N\text{-}A}$. The primary difference with the 8CB +aerosil system is that this behavior is ''stretched'' in ρ_S for

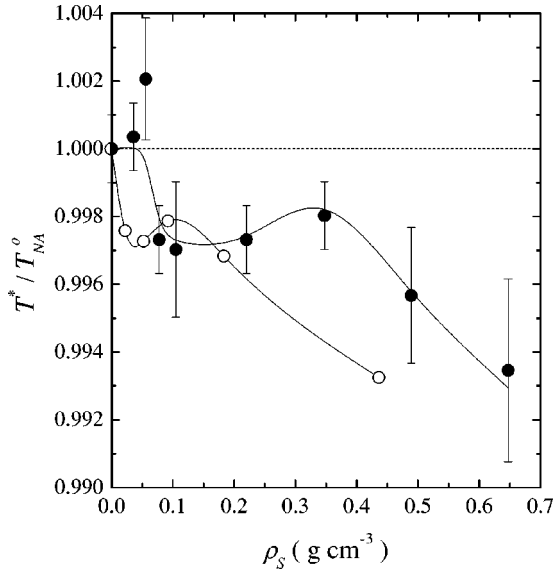

FIG. 5. Dependence on ρ_S of the pseudotransition N–Sm-A temperature T^* scaled by the bulk value for 8OCB+aerosil (solid circles, $T^o_{N\text{-}A}=339.52$ K) and 8CB+aerosil (open circles, $T^o_{N\text{-}A}=306.97$ K) samples. Data for 8CB+aerosil samples taken from Ref. [1]. The solid lines are guides to the eye.

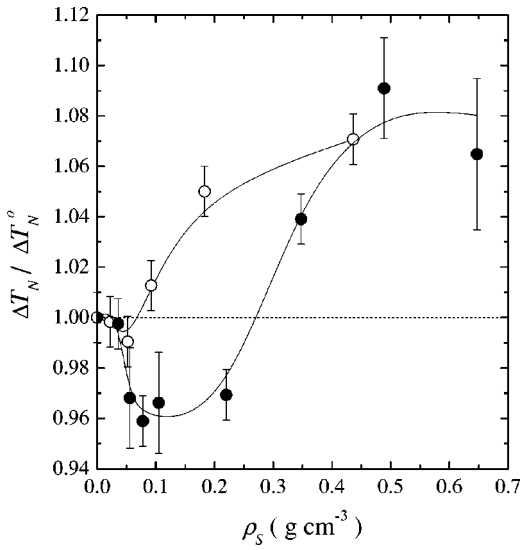

FIG. 6. The nematic phase temperature range $\Delta T_N=T_{I\text{-}N}-T^*$ scaled by the bulk value for 8OCB+aerosil (solid circles, $\Delta T^o_N=12.95$ K) and 8CB+aerosil (open circles, $\Delta T^o_N=7.01$ K) samples. Data for 8CB+aerosil taken from Ref. [1]. The solid lines are guides to the eye.

the 8OCB+aerosil samples. This is consistent with the evolution of $T_{I\text{-}N}$ shown in Fig. 4 and described above.

The nematic phase temperature range, $\Delta T_N=T_{I\text{-}N}-T^*$, normalized by the bulk nematic range $\Delta T^o_N=T^o_{I\text{-}N}-T^o_{N\text{-}A}$, is shown in Fig. 6. While the individual transition temperature changes reflect the absolute stability limit of the nematic and smectic phases, ΔT_N reflects the relative stability of both phases. For 8CB+aerosil, a decrease of $\sim$1% in ΔT_N was seen up to $\rho_S\approx 0.1$, corresponding to the the local maximum of $T_{I\text{-}N}(\rho_S)$ and $T^*(\rho_S)$. This was originally thought to be scatter in the data of Ref. [1]. For 8OCB+aerosil samples, a similar and far more pronounced 4% decrease in ΔT_N is seen from $\rho_S=0.051$ to 0.220. This decrease in ΔT_N reflects a greater depression of $T_{I\text{-}N}$ than T^* and indicates that in this range of silica density, the disorder primarily effects nematic (orientational) ordering. Upon further increasing ρ_S, the nematic range begins to increase and appears to saturate at an 8% increase similar to that seen in the 8CB+aerosil system. This growth in the nematic range occurs because of the greater suppression of T^* relative to $T_{I\text{-}N}$ and so, reflects that above $\rho_S\gtrsim 0.2$, the effect of the silica gel is to mainly disorder smectic (1D-translational) ordering.

The calorimetric results on the I-N transition temperature described above suggest the importance of sample homogeneity. As a test of the fragility of the silica gel, heat capacity scans were performed on a low- and high-density 8OCB +aerosil sample immediately before and after crystallization of the LC. Such a thermal cycle for the $\rho_S=0.051$ sample is shown in Fig. 7 and for the $\rho_S=0.220$ sample in Fig. 8 as a function of $\Delta T=T-T_{I\text{-}N}$ in order to suppress hysteresis effects of the I-N transition. The effect of crystallization on the $\rho_S=0.051$ sample is striking, revealing significant distortion of the ΔC_p signature at both the I-N and N–Sm-A transitions. The appearance of an additional broad ΔC_p feature beginning $\sim$0.9 K below $T_{I\text{-}N}$ as well as a broadened feature

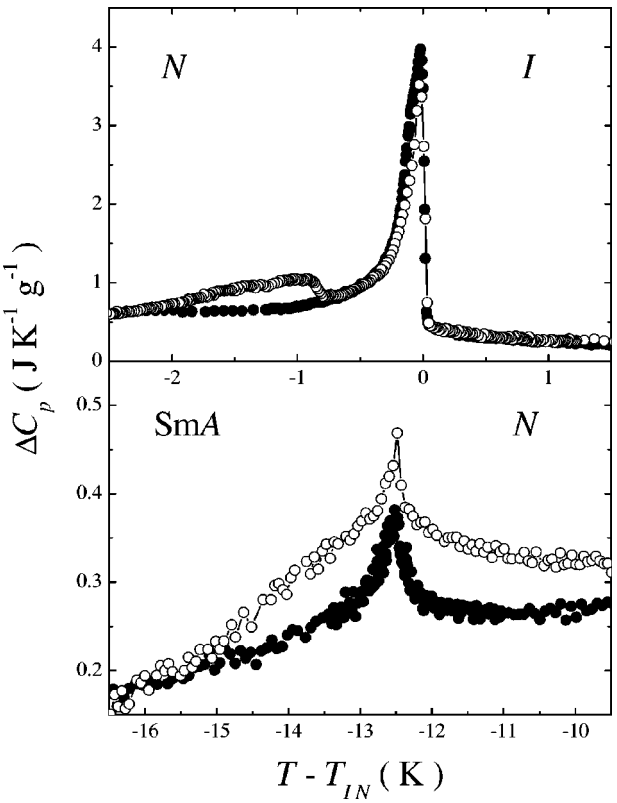

FIG. 7. Behavior of the *I*-*N* and *N*–Sm-*A* excess specific heat of the $\rho_S = 0.051$ sample as a function of temperature relative to $T_{I\text{-}N}$ before (solid circles, $T_{I\text{-}N} = 352.76$ K) and after (open circles, $T_{I\text{-}N} = 352.07$ K) sample crystallization. Both are heating scans made under identical ac-calorimetry conditions. Note the excess enthalpy for the *N*–Sm-*A* transition and the second feature near the *I*-*N* transition as well as a ~0.7 K shift *downward* of $T_{I\text{-}N}$ observed after crystallization. See text for details.

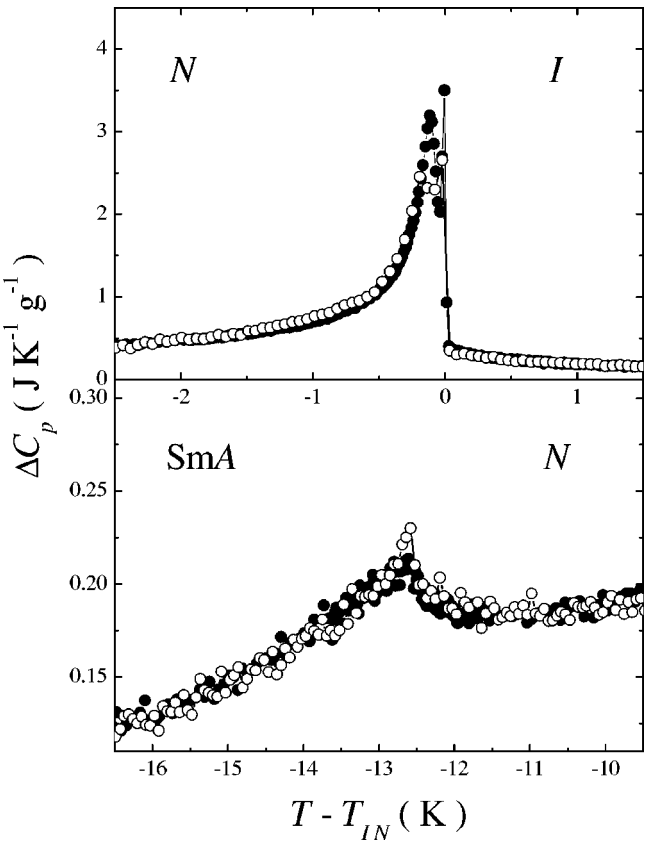

FIG. 8. Behavior of the *I*-*N* and *N*–Sm-*A* excess specific heat of the $\rho_S = 0.220$ sample as a function of temperature about $T_{I\text{-}N}$ before (solid circles, $T_{I\text{-}N} = 351.02$ K) and after (open circles, $T_{I\text{-}N} = 351.23$ K) sample crystallization. The after scan used the same ac-input power but a faster temperature scan rate than the scan before crystallization; both are heating scans. Note the nearly perfect reproducibility of ΔC_p with a $T_{I\text{-}N}$ shift *upward* of ~0.2 K observed after crystallization. See text for details.

over the *N*–Sm-*A* transition region after crystallization may indicate increased sample inhomogeneity, presumably caused by the local expulsion of silica particles as LC crystallites form. However, there are two puzzling aspects: (1) the shift in $T_{I\text{-}N}$ is *downward* by ~0.7 K and (2) the specific distortion seen in ΔC_p about T^* reveals an *increased* *N*-Sm*A* transition enthalpy. The first aspect is counterintuitive as the expulsion of impurities upon crystallization should have moved the system closer to bulk behavior by increasing the size of pure LC domains (regions where no silica is present). The second aspect is particularly puzzling as the *N*–Sm-*A* transition enthalpy after crystallization surpasses the *N*–Sm-*A* transition enthalpy for *bulk* 8OCB ($\Delta H_{N\text{-}A}^{\text{before}} = 0.334$, $\Delta H_{N\text{-}A}^{\text{after}} = 0.65$, and $\Delta H_{N\text{-}A}^{\text{bulk}} = 0.42$ all given in units of J g^{-1}). Visual inspection of the sample immediately after the first crystallization revealed no obvious inhomogeneities. A recent Raman spectroscopy study of 8CB crystallizing within a gel matrix provides evidence of new solid and semisolid phases at low temperature [30]. The additional enthalpy observed here could indicate new solid phases for 8OCB +aerosil samples. These results are only observed upon initial crystallization of a freshly dispersed 8OCB+aerosil sample. Bulk 8OCB behavior is eventually approached upon repeated thermal cycling through the crystallization transition. Clearly, at these low silica densities, the silica gel is, at least locally, quite fragile and short-range restructuring of the gel can strongly affect the liquid crystal.

The results of initial cycling through the crystallization transition for the $\rho_S = 0.220$ sample shown in Fig. 8 do not reveal any significant changes. Aside from a very small, sharp, additional heat capacity feature at the *N*–Sm-*A* transition, the ΔC_p curves are almost perfectly reproducible. The shift in $T_{I\text{-}N}$ after the initial crystallization is small and upward by ~0.2 K, as expected by the expulsion of impurities. This indicates that for higher silica densities, the gel is robust and well behaved. Note that there is no appreciable change in the nematic range, as seen in both Figs. 7 and 8.

IV. DISCUSSIONS AND CONCLUSIONS

Results have been presented from high-resolution ac-calorimetric experiments on 8OCB+aerosil dispersions with emphasis on the weakly first-order *I*-*N* phase transition. These results for 8OCB+aerosil dispersions have been compared with existing results for 8CB+aerosil dispersions [1,2] and reveal new aspects of the effect of quenched random disorder on liquid crystal phase transitions. In particular,

these two LC+aerosil systems are very similar except for the relative elasticity of the LC material. The material 8OCB is elastically stiffer, having an effective (single) nematic elastic constant K_N larger by approximately 20%, than 8CB, and this is reflected by the higher transition temperatures for the nematic, smectic, and crystal phases. Thus, aspects that are LC material dependent and those that are general to quenched random disorder can be distinguished.

From the very good overlap of the ΔC_p wings away from the *I*-*N* two-phase coexistence region and from direct NMR studies on 8CB+aerosil [17] a general feature of LC +aerosils is that the magnitude of the nematic order S is essentially the same as in the bulk LC. Thus, the main effect of QRD is on the director structure with the elasticity of the LC and the kinetics of the ordered phase growth as likely important factors. This is supported by the differences seen between 8OCB+aerosil and 8CB+aerosil systems; in particular, the different ρ_S dependence is likely connected to the difference in elasticity for the two liquid crystals.

The effect of quenched random disorder on first-order phase transitions is substantially different than that on continuous phase transitions. First-order transitions have an additional energy penalty for the formation of interfaces between coexisting phases, which complicates random-field-type theoretical approaches. In the classical treatment, first developed by Imry and Wortis [8], the QRD effect on first-order transitions is that a quenched random-field creates domains having a randomly shifted transition temperature. This would have the effect of smearing the overall transition, a monotonic decrease in the transition latent heat and temperature with increasing QRD, and a low-temperature phase possessing only short-range order for arbitrarily weak QRD. These predictions are generally consistent with the behavior of nematic in aerogels [27]. For nematics in aerosils, the transition latent heat appears to decrease and the width of the coexistence region to increase monotonically with increasing disorder as well as the transition becoming apparently continuous for high disorder strength. These features are generally consistent with the classical picture. However, the character of the transition and the nonmonotonic transition temperature shifts do not appear to be consistent with this view. More strikingly, the *I*-*N* transition in aerosils in some range of ρ_S appears to proceed via two transitions. This could only occur in the classical view if a bimodal distribution of the random-field variance $\langle h^2 \rangle$, connected to a bimodal distribution in ρ_S, is present. This is not supported by SAXS studies, which revealed the fractal-like nature of the aerosil gel structure [1], nor the behavior at the *N*–Sm-*A* transition [1,31,32]. However, nematics are very ''soft'' materials and the QRD imposed by aerosils appears to be much weaker than that of aerogels, thus elasticity of the LC (and possibly the gel) can play an important role.

In LC+aerosil systems, $\langle h^2 \rangle$ is thought to depend on the given concentration of silica and interaction with the LC, whereas the LC elasticity K_N is strongly temperature dependent (being proportional to S^2) near and below $T_{I\text{-}N}$. Since the aerosil gel is thixotropic and formed in the isotropic phase, any high energy strains or deformations that may exist are likely quickly annealed, the anisotropy of the gel should be fixed and essentially zero, especially for rigid gel structures such as aerogels. However, the disordering nature of the gels may evolve with thermal history of the LC in aerosil gels. As seen by the result of cycling through crystallization presented here as well as the DNMR [17] and electro-optical [10,11] studies, the gel can be compliant with respect to distortions in the director structure for a range of silica densities. Note that the quantity $T_{I\text{-}N}$ differs by at most 10% between 8CB and 8OCB thus the energy scales are similar while the twist elastic constant differs by 36%.

The features described above suggests a possible physical scenario for the origin of the double ΔC_p feature at the *I*-*N* (or any ''soft'' first-order [33]) transition in LC+aerosil systems. As the nematic elastic constant strongly increases with decreasing temperature for $T \lesssim T_{I\text{-}N}$, a ''skin'' of low nematic order (due to the undulations of the aerosil strands) may coat the silica strands. The thickness of this paranematic boundary layer would be strongly temperature dependent, shrinking with decreasing T below $T_{I\text{-}N}$. The presence of such a layer would serve to partially decouple the disordering (or field) effect of the silica gel from the void nematic (acting as a kind of ''lubricant''). Once the layer thickness reaches its minimum value (roughly equivalent to a molecular length) the elasticity of the void nematic becomes strongly coupled to that of the aerosil gel. This would effectively increase, for a given ρ_S, the disorder strength.

A consequence of this speculation for a first-order transition induced change in disorder strength (through the onset of coupling between the director fluctuations and gel) would be the alteration of the gel dynamics (i.e., vibrational modes). This would be consistent with large changes in the relaxation times of aerosil gels observed by dynamic x-ray studies on 8CB+aerosil near $T_{I\text{-}N}$ [16]. In addition, this coupling should dampen director fluctuations and could account for the variation in the critical behavior seen at the *N*–Sm-*A* transition for LC+aerosil samples. Another consequence of this view is that the director correlation length $\xi_{\hat{n}}$ (the relevant aspect of nematic order) would jump to a large isotropic value at the first transition and upon further cooling cross a second transition into a more strongly disordered state having a *smaller* correlation length. The isotropic nature of $\xi_{\hat{n}}$ and the final SRO state of the nematic with QRD are consistent with recent optical studies [11] and the detailed evolution of $\xi_{\hat{n}}$ through the two transitions is the subject of current optical and calorimetric study [34].

The different silica density dependence of $T_{I\text{-}N}$ and the temperature distance between the two C_p peaks (δT_{2p}) between 8OCB+aerosil and 8CB+aerosil would also be consistent with the difference in the nematic elasticity of the two liquid crystals. A stiffer silica gel (higher ρ_S) would be required to influence a stiffer LC, thereby stretching the shift in $T_{I\text{-}N}$ with respect to ρ_S as seen between the 8OCB+aerosil and 8CB+aerosil systems. The ρ_S dependence in the high-density regime of δT_{2p} for 8OCB+aerosil (see Table I) compared to the nearly constant $\delta T_{2p} \sim 0.1$ K seen only in the low-density regime of 8CB+aerosil [1] would be compatible with a transition induced increase in the variance of the gel disorder strength. The liquid-crystal 8CB being much softer would only be able to stress a very weak (low ρ_S) gel while

the much stiffer 8OCB would be able to distort a wider range of gels. Since the ρ_S dependence of the critical behavior for the $N-$Sm-A transition is quite similar between 8CB+aerosil and 8OCB+aerosil [4], these observations suggest that the effects observed at the I-N transition are not directly connected to those at the $N-$Sm-A.

Finally, the unexpected behavior of low silica density sample when initially cycled through the crystallization transition is not fully understood. The expulsion of silica impurities by the strongly first-order crystallization transition seems to lead to a *more* disordered system. One possibility to explain this phenomena is that the initial crystallization causes the expulsion of the silica particles locally and transforms the flexible fractal structure into a more rigid, foam-like, gel. The depression of $T_{I\text{-}N}$ is then a consequence of the greater elastic distortions imposed by the new gel arrangement. Repeated cycling through crystallization would continue to expel impurities, eventually destroying the foam-like structure. Once the silica has been compacted sufficiently, percolation is no longer possible and free-floating silica particles would represent an annealed disorder. The gels formed in the high silica density samples are more robust and would not be expected to change significantly when the LC crystallize. This view can be directly tested with a detailed structural study by small-angle x-ray scattering where the thermal history is carefully controlled. The increase in the enthalpy of the $N-$Sm-A transition after the initial crystallization to a value greater than the bulk LC value remains a puzzle. Note that the speculations presented here for the double I-N transition peaks and the unusual hysteresis behavior are intended to motivate future experimental and theoretical studies.

ACKNOWLEDGMENTS

The authors wish to thank C. W. Garland, Robert Leheny, and Tommaso Bellini for many helpful discussions. Funding in Toronto was provided by the Natural Science and Engineering Research Council of Canada, and the work at WPI was supported by the NSF under the NSF-CAREER Grant No. DMR-0092786.

[1] G.S. Iannacchione, C.W. Garland, J.T. Mang, and T.P. Rieker, Phys. Rev. E **58**, 5966 (1998).
[2] G.S. Iannacchione, S. Park, C.W. Garland, R.J. Birgeneau, and R.L. Leheny, Phys. Rev. E **67**, 011709 (2003).
[3] T. Bellini, L. Radzihovsky, J. Toner, and N.A. Clark, Science **294**, 1074 (2001), and references therein.
[4] P.S. Clegg, C. Stock, R.J. Birgeneau, C.W. Garland, A. Roshi, and G.S. Iannacchione, Phys. Rev. E **67**, 021703 (2003).
[5] P. G. de Gennes and J. Prost, *The Physics of Liquid Crystals*, 2nd ed. (Clarendon Press, Oxford, England, 1993).
[6] M. J. P. Gingras (private communication).
[7] D.E. Feldman, Phys. Rev. Lett. **84**, 4886 (2000).
[8] Y. Imry and M. Wortis, Phys. Rev. B **19**, 3580 (1979).
[9] T. Bellini, N.A. Clark, V. Degiorgio, F. Mantegazza, and G. Natale, Phys. Rev. E **57**, 2996 (1998).
[10] T. Bellini, M. Buscaglia, C. Chiccoli, F. Mantegazza, P. Pasini, and C. Zannoni, Phys. Rev. Lett. **85**, 1008 (2000).
[11] T. Bellini, M. Buscaglia, C. Chiccoli, F. Mantegazza, P. Pasini, and C. Zannoni, Phys. Rev. Lett. **88**, 245506 (2002).
[12] B. Zhou, G.S. Iannacchione, C.W. Garland, and T. Bellini, Phys. Rev. E **55**, 2962 (1997).
[13] M. Marinelli, A.K. Ghosh, and F. Mercuri, Phys. Rev. E **63**, 061713 (2001).
[14] S. Park, R.L. Leheny, R.J. Birgeneau, J.-L. Gallani, C.W. Garland, and G.S. Iannacchione, Phys. Rev. E **65**, 050703(R) (2002).
[15] R.L. Leheny, S. Park, R.J. Birgeneau, J.L. Gallani, C.W. Garland, and G.S. Iannacchione, Phys. Rev. E **67**, 011708 (2003).
[16] C. Retsch, I. McNulty, and G.S. Iannacchione, Phys. Rev. E **65**, 032701 (2002).
[17] T. Jin and D. Finotello, Phys. Rev. Lett. **86**, 818 (2001).
[18] J.D. Litster, J. Als-Nielsen, R.J. Birgeneau, S.S. Dana, D. Davidov, F. Garcia-Golding, M. Kaplan, C.R. Safinya, and R. Schaetzing, J. Phys. Colloq. **40**, C3 (1979).
[19] M.J. Bradshaw, E.P. Raynes, J.D. Bunning, and T.E. Faber, J. Phys. (France) **46**, 1513 (1985).
[20] Degussa Corp., Silica Division, 65 Challenger Road, Ridgefield Park, NJ 07660. Technical data are given in the Degussa booklet AEROSILS.
[21] H. Yao and C.W. Garland, Rev. Sci. Instrum. **69**, 172 (1998).
[22] The correction factors are, explicitly, $f(\omega)=[1+\cos^2(\varphi)\times(2R_i/3R_e+2\tau_i/\tau_e-2\tau_s\tau_c\omega^2)]^{-1/2}$ and $g(\omega)=f(\omega)[1+\omega\tau_i/\tan(\varphi)]$ where the internal thermal relaxation time is the sum of that for the sample and cell, $\tau_i=\tau_s+\tau_c$, and the external thermal relaxation time is given by $\tau_e=R_eC$. In the limit of zero internal thermal resistance, or $\tau_i \ll \tau_e$, both $f(\omega)$ and $g(\omega)$ approach 1 for all ω.
[23] Isotherm frequency scans performed on our sample+cell configuration find an internal thermal relaxation time of $\tau_i \lesssim 1.5$ sec. Also, the thermal diffusion length of the sample is approximately a factor of 2 larger than the thickness of the sample at the heating period of 42.7 sec. Thus, the sample +cell configuration employed in this study can be reasonably modeled as a single thermal mass having negligible internal temperature gradients.
[24] G.B. Kasting, K.J. Lushington, and C.W. Garland, Phys. Rev. B **22**, 321 (1980).
[25] R.J. Birgeneau, C.W. Garland, G.B. Kasting, and B.M. Ocko, Phys. Rev. A **24**, 2624 (1981).
[26] For a sample+cell configuration describable as a single thermal mass and in a one-phase region of the sample material, the complex heat capacity should be purely real, i.e., $C''=0$, in the absence of dynamics. This is usually the case given the low operating frequencies employed in our calorimeters and confirmed by $C''=0$ through all second-order phase transitions studied. The situation changes for a first-order transition where presumably the evolution of the latent heat in the two-phase region introduces a second oscillating heat source due to the oscillating temperature. It is reasonable to picture this internal source operating in the two-phase coexistence region as inco-

herent with the applied oscillating heat to the cell and thus it should add to the total phase shift. The result is a phase shift peak at a first-order phase transition.

[27] L. Wu, B. Zhou, C.W. Garland, T. Bellini, and D.W. Schaefer, Phys. Rev. E **51**, 2157 (1995).

[28] A very small feature whose exact origin is unclear but may reflect an annealed impurity is seen in bulk at $\Delta T = T - T_{N\text{-}I} \approx -0.5$ K and shifts upward relative to $T_{N\text{-}I}$ for the $\rho_S = 0.036$ sample.

[29] P. Jamee, G. Pitsi, and J. Thoen, Phys. Rev. E **66**, 021707 (2002).

[30] C. Fehr, P. Dieudonne, J.L. Sauvajol, and E. Anglaret, Phys. Rev. E **67**, 061706 (2003).

[31] H. Haga and C.W. Garland, Liq. Cryst. **23**, 645 (1997).

[32] H. Haga and C.W. Garland, Phys. Rev. E **56**, 3044 (1997).

[33] In fact, double C_p peaks were observed at the $N-$Sm-A transition in 7O.4+aerosil samples, which is first order due to the proximity of the I-N transition. See H. Haga and C.W. Garland, Liq. Cryst. **23**, 645 (1997).

[34] T. Bellini, F. Mantegazza, A. Roshi, and G. Iannacchione (unpublished).